CHEMNANOMAT

CHEMISTRY OF NANOMATERIALS FOR ENERGY, BIOLOGY AND MORE

www.chemnanomat.org

Accepted Article

Title: Exploiting hydrogen bonding to direct supramolecular polymerization at the air/water interface

Authors: Pablo G. Argudo, João Paulo Coelho, Irene López-Sicilia, Andrés Guerrero-Martínez, María T. Martín-Romero, Luis Camacho, Gustavo Fernández, and Juan José Giner-Casares

To be cited as: *ChemNanoMat* **2022**, e202200448

Link to VoR: https://doi.org/10.1002/cnma.202200448

A Journal of

ACES Asian Chemical Editorial Society

A sister journal of **Chemistry – An Asian Journal** and **Asian Journal of Organic Chemistry**

WILEY-VCH

10.1002/cnma.202200448

WILEY-VCH

RESEARCH ARTICLE

Exploiting hydrogen bonding to direct supramolecular polymerization at the air/water interface

Pablo G. Argudo,[a] João Paulo Coelho,*[b] Irene López-Sicilia,[a] Andrés Guerrero-Martínez,[c] María T. Martín-Romero,[a] Luis Camacho,[a] Gustavo Fernández,*[b] Juan J. Giner-Casares*[a]

[a] Dr. Pablo G. Argudo, M. Sc. Irene López-Sicilia, Prof. María T. Martín-Romero, Prof. Luis Camacho, Prof. Juan J. Giner Casares
Departamento de Química Física y T. Aplicada, Instituto Universitario de Nanoquímica IUNAN, Facultad de Ciencias, Universidad de Córdoba (UCO), Campus de Rabanales, Ed. Marie Curie, E-14071 Córdoba, Spain.
E-mail: jjginer@uco.es
[b] Dr. João Paulo Coelho, Prof. Gustavo Fernández
Organisch-Chemisches Institut, Westfälische Wilhelms-Universität Münster, Corrensstraße 36, 48149 Münster, Germany.
E-mail: jpaulogaio@gmail.com (J. P. C.), fernandg@uni-muenster.de (G.F.)
[c] Departamento de Química Física I, Universidad Complutense de Madrid, Avda. Complutense s/n, 28040 Madrid, Spain.
Supporting information for this article is given via a link at the end of the document.

Abstract: Fluid interfaces provide an advanced platform for directed self-assembly of organic composites and formation of supramolecular polymers (SPs). Intermolecular interactions govern the supramolecular polymerization processes, with hydrogen bonding (H-bonding) as a key interaction in supramolecular chemistry and biology. Two purposefully designed supra-amphiphiles for assessing the role of H-bonding were designed and their supramolecular polymerization (SP) at the air/water interface was compared. H-bonding was confirmed by in situ experimental and computational techniques as the required intermolecular interaction for attaining SPs with well-defined molecular arrangement. Control of H-bonding as opposite to traditionally considered interactions, e.g., π-π stacking is proposed as a successful strategy for SP at fluid interfaces.

Introduction

Supramolecular chemistry at interfaces allows a delicate interplay between intermolecular interactions.[1,2] A broad array of two-dimensional (2D) materials can be obtained via interfacial self-assembly.[3–5] Air/liquid interfaces are highly relevant in this sense, allowing a high degree of conformational freedom and intermolecular interactions between the molecules located at the interface.[6,7] In this regard, supramolecular polymers (SPs) are highly versatile materials with multiple applications.[8] While solid/liquid and liquid/liquid interfaces have been used for obtaining SPs at interfaces, whereas air/liquid interfaces remain a promising platform in this sense.[9–12]

Hydrogen bonding interactions (H-bonding) are commonly used directional non-covalent forces for directing self-assembly processes, both in solution and in bulk conditions.[13–15] In addition, H-bonding at the air/water interface has been successfully applied to monolayers of surfactants with complex headgroups for sustaining the 2D crystalline structure.[16] For instance, urea groups have been included in derivatives of phospholipids for promoting the formation of intermolecular H-bonds, thus reaching a new condensed phase.[17]

Hydration effects are widely known to have a large impact on supramolecular self-assembly.[18,19] We thus envisaged the confinement of amphiphilic monomers for supramolecular polymerization (SP) at a hydrophobic/hydrophilic interface, i.e., air/water interface, as a relevant strategy to control hydration, self-assembly, and H-bonding.[20] Moreover, such interfacial self-assembly should provide high predictability of the formed SPs, given that the process would be exclusively triggered by mechanical stimulus.[21] Note that supramolecular polymerization involve reversible, non-covalent intermolecular interactions and ordering of the monomers, as opposed for classical polymerization in which covalent bonds are formed between monomers. Hydrophilic PEGylation of exclusively one phenyl ring and substitution with hydrophobic alkyl chains of the opposite phenyl ring are reported strategies to obtain amphiphilic monomers for self-assembly.[22–24]

Results and Discussion

In this work, we examine the role of directional H-bonding interactions in SP at the air/water interface. To this end, we designed two discrete amphiphilic derivatives **1** and **2** that differ in the absence or presence of H-bonding synthons (Figure 1A, for synthesis and characterization, see the Supporting Information (S.I.) and the report from Percec et al.[25]). The trisubstitution of the peripheral benzene rings with alkoxy or ethylene glycol chains is a common structural element of multiple examples of monomers undergoing SP. For both derivatives, solvophobic interactions and π–stacking[26,27] are expected to play an important role at the air/water interface. While derivative 1 features an alkyne spacer between the two aromatic rings, derivative 2 comprises an amide group included to promote self-assembly into well-defined SPs via H-bonding. Note that alternative chemical groups, e. g., ester group or methylated amide groups might also be of relevance for studying the intermolecular H-bonding.

10.1002/cnma.202200448

WILEY-VCH

RESEARCH ARTICLE

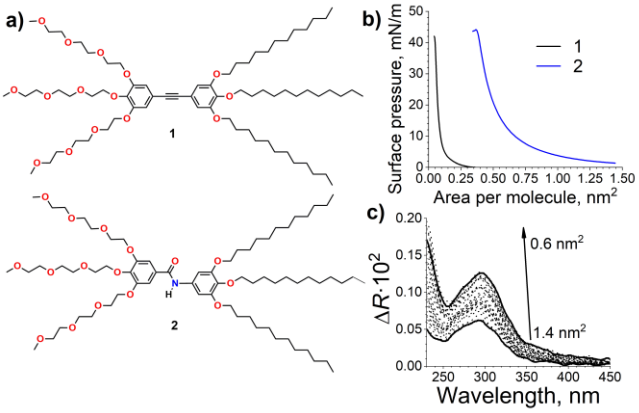

Figure 1. (a) Molecular structure of amphiphilic derivatives **1** and **2**. (b) Surface pressure-molecular area isotherms of **1** and **2** at the air/water interface. (c) In situ UV-vis reflection spectra of **2** at the air/water interface. The area values per molecule are noted in the inset.

Both **1** and **2** derivatives displayed amphiphilic character, forming monolayers at the air/water interface (Figure 1B). Each molecule formed a monolayer film and was compressed and expanded using the mechanical stimulus provided by the Langmuir technique with no significant hysteresis (see Figures S3, S4). Compounds **1** and **2** formed stable films at the air/water interface, with a collapse surface pressure above 40 mN·m^{-1}. Remarkably, significantly different areas per molecule were obtained. The isotherm for **1** showed a lower than expected limiting area of ca. 0.1 nm^2 per molecule, while a final value of 0.6 nm^2 would be expected for a completely upright conformation of the three alkyl chains.[28] Thus, some loss of molecules to the subphase after spreading and prior to compression is expected, given the full recovery in the isotherms (Figure S3). In contrast, the limiting area in the isotherm of **2** by extrapolating the linear region of the isotherm at high surface pressure to the intercept at 0 mN/m was ca. 0.6 nm^2 per molecule, in full agreement with the expected value considering a tight packing of **2** at the air/water interface.

The extent of aromatic interactions was monitored by in situ UV-vis reflection spectroscopy at the air/water interface.[29] Amide derivative **2** displayed a UV-vis reflection peak centered at ca. 295 nm (Figure 1C). The UV-vis reflection signal increased with decreasing available surface area per molecule, indicating the persistence of molecules of **2** at the monolayer on the air/water interface and further confirming the amphiphilic character of **2**. Similar results were obtained for **1**, with a UV-vis reflection peak at ca. 303 nm (Fig. S5). The comparatively low UV-vis reflection signal of **1** might originate from a certain non-ordered aggregation of the monomers of **1** into the subphase upon completion of a monolayer, which is highly stable and reproducible according to the isotherms in Figure S3 as mentioned above. A certain fraction of **1** was dispersed into the water subphase, probably as aggregates with the poly(ethylene glycol) providing the outer hydrophilic surface. Once the stable amount of **1** is present at the air/water interface after spreading, the monolayer is highly stable. The UV-vis reflection data also provided insights on the aggregation of the aromatic rings through variations in the maximum value of the reflection intensity (ΔR_{max}) at different values of surface concentration (Figure 2A,C). While **1** displayed an increase of the intensity with a maximum value at early stages of compression, a steady and lineal growth of the intensity was observed for **2** up to a limiting value of ΔR_{max} = 0.13.

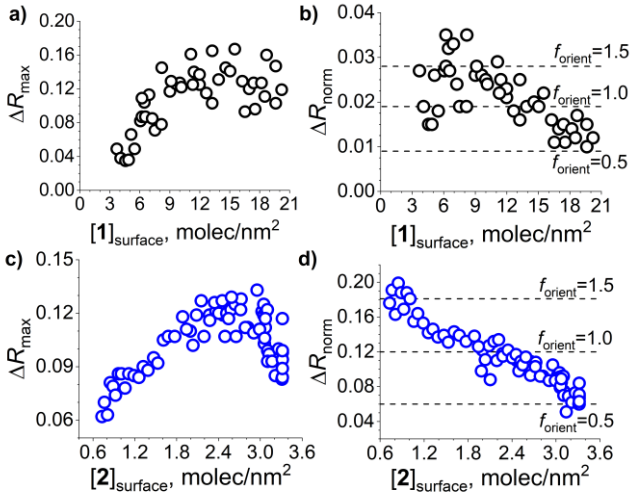

Figure 2. (a) Maximum value of the UV-vis reflection spectra of **1** at the air/water interface at different surface concentrations. (b) Values of normalized UV-vis reflection spectra (ΔR_{norm} = ΔR·A) of **1** at the air/water interface at different surface concentrations. Relevant values of the orientation factor (f_{orient}) are included for reference. (c) Maximum value of the UV-vis reflection spectra of **2** at the air/water interface at different surface concentrations. (d) Values of normalized UV-vis reflection spectra (ΔR_{norm} = ΔR·A) of **2** at the air/water interface at different surface concentrations. Boundary values of the orientation factor (f_{orient}) are included for reference.

From equation (1), the normalized UV-vis reflection intensity (ΔR_{norm}) could be obtained:

$$\Delta R_{norm} = \Delta R \cdot A \qquad (1)$$

where A is the area per molecule. The variation of ΔR_{norm} with the surface concentration of the derivatives (1/*A*) provided information on the relative orientation of the transition dipole of the aromatic core of the molecules with respect to the water surface, according to equation (2):

$$\Delta R_{norm} = 5.41 \cdot 10^6 \cdot f_{orient} \cdot \varepsilon \qquad (2)$$

where ε is the molar extinction coefficient ε = 5.41·10^6 M^{-1}·cm^{-1} from the UV-vis reflection spectra at high values of area per molecule of **2**, in agreement with the bulk UV-vis spectrum. f_{orient} is the orientation factor. Values of the orientation factor f_{orient} = 1.5, 1.0, and 0.5 correspond to parallel, random, and perpendicular orientations of the transition dipole of the aromatic core with respect to the water surface, respectively.

The orientation factor of **1** suggested gradually varying orientation at almost any surface concentration, with most of the UV-vis reflection spectra a random orientation with values of f_{orient} scattered around **1** (Figure 2B). In contrast, the molecular ordering of **2** increases upon decreasing the available surface area (see Figure 2D), starting from a parallel arrangement with respect to the water surface, at f_{orient} = 1.5, and reaching a perpendicular arrangement when highly compressed at f_{orient} = 0.5. This perpendicular arrangement of the aromatic groups with

10.1002/cnma.202200448

respect to the air/water interface was in agreement with the molecular area observed for **2** (see Figure 1B). Despite that the variation of the orientation of **1** and **2** with compression is similar, the arrangement of **1** shows a significantly more scattered shift of the UV-vis reflection peak, in contrast to the well-defined shift for **2**. These UV-vis spectroscopy results suggest aggregation and local modification of the dielectric environment for **1** and a well-defined process of SP for **2** (Figure S6).[30] The values of the tilt angle of the transition dipole of the aromatic core were calculated from the values of the orientation factor, further confirming this behavior (Figure S7). Therefore, the formation of SPs of **2** with well-defined molecular arrangement at the air/water interface was supported by the UV-vis reflection spectra.

The morphology of the aggregates was observed in situ at the air/water interface by Brewster Angle Microscopy (BAM).[31] The BAM pictures for molecule **1** remained rather homogenous during the compression process (Figure S8); only some bright small dots appeared, probably corresponding to solid-like aggregates of **1**, in agreement with the UV-vis reflection data. The BAM pictures for the monolayer of **2** displayed a completely homogenous morphology during compression at large values of area per molecule (Figure S9). However, twisted and spiral-like aggregates with sizes of several microns appeared at reduced surface area values of ca. 0.3 nm^2 per molecule (Figure 3). The aggregates of **2** were composed of anisotropic ordered molecules forming the SPs.[32]

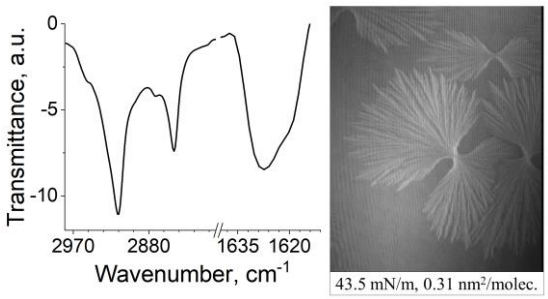

Figure 3. (Left) FTIR spectra of 32 monolayers of **2** transferred onto a CaF_2 substrate showing the CH_2 stretching region (right) and the C=O stretching band (left). (Right) Brewster Angle Microscopy picture of SPs of **2** recorded at the air/water interface. The value of the surface pressure and area per molecule is noted in the inset.

The formation of these SPs is promoted by the amide group of **2**, given the absence of any SP in **1**. Note that, with successive cycles of compression and expansion, the SPs at the interface formed grain-like domains of comparatively smaller sizes for the second cycle, while only a small fraction of bright dots was observed during the third cycle (Figure S10). This morphological change might point to a certain memory effect of the SPs even after disassembly promoted by the H-bonds in **2**. The ordered structures at microscopic level were observed exclusively in the first cycle and might contain solid-like nuclei that persisted as the observed bright dots during the second and third cycles. The compression to the quasi-collapse region of the monolayer required to obtain the observed SPs might indicate a thermodynamic barrier that can be surmounted by applying a mechanical stimulus to the film formed by **2**.[33]

The formation of H-bonds was confirmed by ex-situ FTIR spectra (Figure 3). Thirty-two monolayers of **2** were transferred onto a CaF_2 solid substrate at 30 $mN \cdot m^{-1}$ to obtain adequate signal-to-noise ratios. Note that this region of the isotherm shows highly packed structures. This packing avoids collapse of the film disrupting the LS transfer by local perturbation in the monolayer induced by the transfer process. Therefore, the LS transfer for ex-situ FTIR measurements was performed at 30 mN/m.

The carbonyl stretching band was located at ca. 1626 cm^{-1}, with a shoulder at ca. 1620 cm^{-1}. These values of frequency were in agreement with the participation of the amide group of **2** in strong H-bonding.[34] The physical state of the alkyl chains of **2** was assessed by the position of the IR bands corresponding to the methylene units. The symmetric and asymmetric vibrational modes of the methylene groups were found at 2850 and 2919 cm^{-1}, respectively. These values correspond to the alkyl chains in all-trans conformation, confirming the tightly packed arrangement.

Molecular dynamics (MD) simulations were performed to gain further insights on the self-assembly process and the final SPs.[35] Thirty-two molecules were placed at the air/water interface on a compressed scenario of 0.59 nm^2 per molecule (Figures 4A and S11). A clearly ordered distribution in slabs of triethylene glycol (TEG) chains, aromatic groups, and hydrophobic chains was obtained (Figure 4B). The minimum in the water distribution indicated a relatively dehydrated region.[36] This narrow region of ca. 0.5 nm corresponds to the transition between the TEG chains and the amide group, both establishing H-bonds with surrounding water molecules. The local dehydration might be ascribed to the competition of the mentioned groups to bind water molecules. The MD simulations suggested that the H-bonds are directing the formation of well-defined SPs sustained mainly by the amide groups (Figures 4C and S12). Note that the formation and exchange of H-bonds is a dynamic process and Figure 4C shows a snapshot. The radial distribution function of NH-to-O atoms further confirmed the significant formation of H-bonding with a maximum at ca. 0.19 nm.[37]

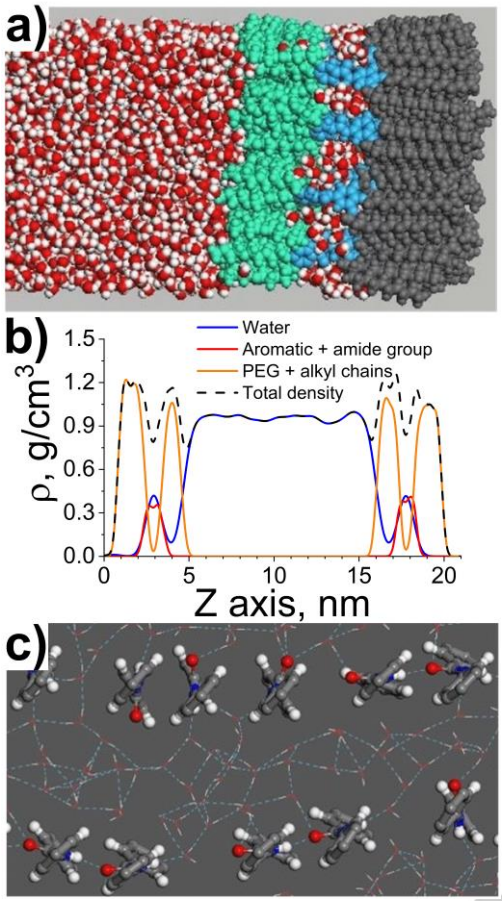

Figure 4. (a) Snapshot of the MD simulations of monolayer of **2**, side view. Green: TEG, blue: amide group, grey: alkyl chains. (b) Atomic distribution density of water, aromatic + amide groups, TEG + alkyl chain groups, and total atomic density in the monolayer of **2**. (c) Top view of the monolayer of **2** showing the formation of H-bonds as dashed blue lines. Nitrogen and oxygen atoms are displayed in blue and red, respectively.

A hexagonal distribution of the hydrophobic chains was observed, as expected for alkyl chains in a highly packed and ordered structure (Figure S13). This agrees with the values obtained for the order parameter (P_{ord}), defined by equation (3):

$$P_{\text{ord}} = \left\langle \frac{3\cos^2\theta_n - 1}{2} \right\rangle \qquad (3)$$

A value of P_{ord} = 1.0 is interpreted as a fully perpendicular orientation of the alkyl chains with respect to the air/water interface, while a value of 0 indicates a random orientation of the tail with respect to the z axis (Figure S14). A high degree of order was obtained, in agreement with the previously observed tight packing of **2** molecules at the air/water interface.

Conclusion

In summary, two structurally related amphiphilic derivatives (**1** and **2**) featuring nonpolar dodecyloxy chains on one molecule end and water-soluble TEG chains on the opposite end were purposefully designed for directed self-assembly at air/water interfaces. Our molecular design allows for multiple interactions upon interfacial SP, including chain immiscibility along with aromatic, hydrophobic interactions, and H-bonding. Interestingly, the presence of an additional amide group for **2**, which is lacking for **1**, allowed us to rationalize the effect of hydrogen bonding on SP processes at air/water interfaces. While the intermolecular interactions of **1** produced a stable film at the air/water interface, the existence of an amide group in **2** resulted in a well-defined supramolecular structure under mechanical stimulus. The obtained molecular arrangement has been comprehensively characterized by a combination of experimental and computational data, demonstrating that directional interactions can induce large differences in the outcome of SP at the air/water interface. Our strategy contributes to broaden the scope of applicability of amphiphilic self-assembled systems, ranging from interfacial self-assembly to fluid and solid interfaces and paves the way for further investigation including additional chemical groups for promoting intermolecular interactions.

Experimental Section

Experimental information, synthesis of derivative 1, surface pressure-molecular area isotherms, UV-vis reflection spectra, Brewster Angle Microscopy pictures, and computational studies.

Acknowledgements

This work has been funded by the Spanish Ministry of Science and Innovation (AEI, Spain, PID2020-112744GB-I00 / AEI /10.13039/501100011033 and RTI2018-095844-B-I00) and the Madrid Regional Government (grant P2018/NMT-4389). Dr. João Paulo Coelho thanks the Alexander von Humboldt foundation for funding. I. López-Sicilia acknowledges the Ministry of Science and Innovation for a FPI predoctoral contract (PRE2021-097546).

Keywords: Supramolecular polymers • Self-assembly • Air/water interface • Surface-pressure • Hydrogen bond

[1] P. Gu, G. Xie, P. Y. Kim, Y. Chai, X. Wu, Y. Jiang, Q. Xu, F. Liu, J. Lu, T. P. Russell, *Angew. Chem. Int. Ed.* **2021**, *60*, 2871–2876.

[2] I. Robayo-Molina, A. F. Molina-Osorio, L. Guinane, S. A. M. Tofail, M. D. Scanlon, *J. Am. Chem. Soc.* **2021**, *143*, 9060–9069.

[3] Q. Guo, X. Zhang, F. Zhao, Q. Song, G. Su, Y. Tan, Q. Tao, T. Zhou, Y. Yu, Z. Zhou, C. Lu, *ACS Nano* **2020**, *14*, 2788–2797.

[4] Z.-F. Cai, G. Zhan, L. Daukiya, S. Eyley, W. Thielemans, K. Severin, S. De Feyter, *J. Am. Chem. Soc.* **2019**, *141*, 11404–11408.

[5] H. Chen, W. Zhang, S. Ren, X. Zhao, Y. Jiao, Y. Wang, J. F. Stoddart, X. Guo, *Adv. Mater.* **2021**, 2101487.

[6] S. Schrettl, C. Stefaniu, C. Schwieger, G. Pasche, E. Oveisi, Y. Fontana, A. F. i Morral, J. Reguera, R. Petraglia, C. Corminboeuf, G. Brezesinski, H. Frauenrath, *Nat. Chem.* **2014**, *6*, 468–476.

[7] J. F. Neal, W. Zhao, A. J. Grooms, M. A. Smeltzer, B. M. Shook, A. H. Flood, H. C. Allen, *J. Am. Chem. Soc.* **2019**, *141*, 7876–7886.

[8] S. Chen, R. Costil, F. K. Leung, B. L. Feringa, *Angew. Chem. Int. Ed.* **2021**, *60*, 11604–11627.

[9] B. Qin, J.-F. Xu, X. Zhang, *Langmuir* **2022**, *38*, 4157–4163.

[10] S. Maji, A. Das, P. K. Sarkar, A. Metya, S. Ghosh, S. Acharya, *RSC Adv.* **2014**, *4*, 44650–44653.

[11] P. Mondal, G. Manna, T. Kamilya, M. Das, K. Ariga, G. J. Richards, J. P. Hill, S. Acharya, *Adv. Mater. Interfaces* **2022**, *9*, 2200209.

[12] S. Biswas, G. Manna, B. Das, A. Bhattacharya, A. K. Pal, A. Datta, P. Alam, I. R. Laskar, P. Mondal, M. K. Mukhopadhyay, M. K. Sanyal, S. Acharya, *Small* **2021**, *17*, 2103212.

[13] C. Naranjo, Y. Dorca, G. Ghosh, R. Gómez, G. Fernández, L. Sánchez, *Chem. Commun.* **2021**, *57*, 4500–4503.

[14] I. Helmers, G. Ghosh, R. Q. Albuquerque, G. Fernández, *Angew. Chem. Int. Ed.* **2021**, *60*, 4368–4376.

[15] R. Madueno, M. T. Räisänen, C. Silien, M. Buck, *Nature* **2008**, *454*, 618–621.

[16] T. Mukhina, G. Brezesinski, C. Shen, E. Schneck, *J. Colloid Interface Sci.* **2022**, *615*, 786–796.

[17] F. Neuhaus, D. Mueller, R. Tanasescu, C. Stefaniu, P.-L. Zaffalon, S. Balog, T. Ishikawa, R. Reiter, G. Brezesinski, A. Zumbuehl, *Soft Matter* **2018**, *14*, 3978–3986.

[18] N. Fukaya, S. Ogi, M. Kawashiro, S. Yamaguchi, *Chem. Commun.* **2020**, *56*, 12901–12904.

[19] S. Ogi, N. Fukaya, Arifin, B. B. Skjelstad, Y. Hijikata, S. Yamaguchi, *Chem. Eur. J.* **2019**, *25*, 7303–7307.

[20] W. Geng, D. Zhang, C. Gong, Z. Li, K. M. Barraza, J. L. Beauchamp, D. Guo, X. Zhang, *Angew. Chem. Int. Ed.* **2020**, *59*, 12684–12688.

[21] J. P. Coelho, M. J. Mayoral, L. Camacho, M. T. Martín-Romero, G. Tardajos, I. López-Montero, E. Sanz, D. Ávila-Brande, J. J. Giner-Casares, G. Fernández, A. Guerrero-Martínez, *J. Am. Chem. Soc.* **2017**, *139*, 1120–1128.

[22] F. Setaro, J. W. H. Wennink, P. I. Mäkinen, L. Holappa, P. N. Trohopoulos, S. Ylä-Herttuala, C. F. van Nostrum, A. de la Escosura, T. Torres, *J. Mater. Chem. B* **2020**, *8*, 282–289.

[23] E. Kostyurina, J. U. De Mel, A. Vasilyeva, M. Kruteva, H. Frielinghaus, M. Dulle, L. Barnsley, S. Förster, G. J. Schneider, R. Biehl, J. Allgaier, *Macromolecules* **2022**, *55*, 1552–1565.

[24] K. Bansal, D. Webster, M. Quadir, *Langmuir* **2022**, *38*, 2066–2075.

[25] V. Percec, D. A. Wilson, P. Leowanawat, C. J. Wilson, A. D. Hughes, M. S. Kaucher, D. A. Hammer, D. H. Levine, A. J. Kim, F. S. Bates, K. P. Davis, T. P. Lodge, M. L. Klein, R. H. DeVane, E. Aqad, B. M. Rosen, A. O. Argintaru, M. J. Sienkowska, K. Rissanen, S. Nummelin, J. Ropponen, *Science* **2010**, *328*, 1009–1014.

[26] Y. Dorca, R. Sánchez-Naya, J. Cerdá, J. Calbo, J. Aragó, R. Gómez, E. Ortí, L. Sánchez, *Chem. Eur. J.* **2020**, *26*, 14700–14707.

[27] Q. Wang, Y. Zhong, D. P. Miller, X. Lu, Q. Tang, Z.-L. Lu, E. Zurek, R. Liu, B. Gong, *J. Am. Chem. Soc.* **2020**, *142*, 2915–2924.

[28] R. T. Rodrigues, J. R. Siqueira, L. Caseli, *J. Colloid Interface Sci.* **2021**, *589*, 568–577.

[29] C. Rubia-Payá, G. De Miguel, M. T. Martín-Romero, J. J. Giner-Casares, L. Camacho, *Adv. Colloid Interface Sci.* **2015**, *225*, 134–145.

[30] P. G. Argudo, M. Carril, M. T. Martín-Romero, J. J. Giner-Casares, C. Carrillo-Carrión, *Chem. Eur. J.* **2019**, *25*, 195–199.

[31] C. Roldán-Carmona, J. J. Giner-Casares, M. Pérez-Morales, M. T. Martín-Romero, L. Camacho, *Adv. Colloid Interface Sci.* **2012**, *173*, 12–22.

[32] I. Schachter, R. O. Paananen, B. Fábián, P. Jurkiewicz, M. Javanainen, *J. Phys. Chem. Lett.* **2022**, *13*, 1307–1313.

[33] J. B. Kelber, A. Bensalah-Ledoux, S. Zahouani, B. Baguenard, P. Schaaf, A. Chaumont, S. Guy, L. Jierry, *Angew. Chem. Int. Ed.* **2020**, *59*, 23283–23290.

[34] G. Socrates, *Infrared and Raman Characteristic Group Frequencies*, Wiley, **2004**.

[35] A. M. Garcia, M. Melchionna, O. Bellotto, S. Kralj, S. Semeraro, E. Parisi, D. Iglesias, P. D'Andrea, R. De Zorzi, A. V. Vargiu, S. Marchesan, *ACS Nano* **2021**, *15*, 3015–3025.

[36] M. Xue, H. Qiu, C. Shen, Z. Zhang, W. Guo, *J. Phys. Chem. Lett.* **2022**, *13*, 4815–4822.

[37] C.-Y. Li, J.-B. Le, Y.-H. Wang, S. Chen, Z.-L. Yang, J.-F. Li, J. Cheng, Z.-Q. Tian, *Nat. Mater.* **2019**, *18*, 697–701.

10.1002/cnma.202200448

WILEY-VCH

RESEARCH ARTICLE

Entry for the Table of Contents

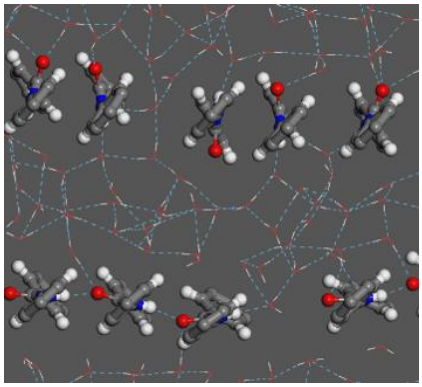

A small detail makes a big difference: by introducing an amide group in self-assembling monomers, directed formation of supramolecular polymers driven by Hydrogen-bonds was achieved at the air/liquid interface.

Institute and/or researcher Twitter usernames: @jj_giner, @Fac_CienciasUCO, @GeciRseq, @CordobaCiencia